

## OVERVIEW NO. 66

# ON MEASURING THE ELASTIC AND DAMPING CONSTANTS OF ORTHOTROPIC SHEET MATERIALS

M. E. MCINTYRE<sup>1</sup> and J. WOODHOUSE<sup>2</sup>

<sup>1</sup>Department of Applied Mathematics and Theoretical Physics, Silver Street, Cambridge CB3 9EW and

<sup>2</sup>Department of Engineering, Trumpington Street, Cambridge CB2 1PZ, England

(Received 21 July 1987)

**Abstract**—Many common sheet materials, ranging from natural materials such as wood to modern composites, possess approximately orthotropic symmetry. Within the approximations of thin-plate bending theory, the linear vibrational properties of such sheets are governed by four elastic constants and four damping constants (at any given frequency). A simple procedure is presented whereby all four elastic constants may be determined, quickly and with reasonable accuracy, from measurements of the resonant frequencies of low-frequency modes of thin rectangular plates with free edges. Also, at least three of the four damping constants may be determined by measuring the damping factors of the same modes—it turns out that the fourth damping constant does not usually have sufficient influence on the low-frequency modes for a reliable value to be found by this approach. The procedure is illustrated with measurements on a range of different sheet materials: wooden plates cut at different angles from the solid timber, plywood, and two very different fibre-reinforced composites. The discussion of these experimental results suggests that this simple procedure could form a valuable part of any programme of quality control, material selection or non-destructive testing involving orthotropic sheet materials.

**Résumé**—De nombreux matériaux lamellaires courants (allant de matériaux naturels, tels que le bois, aux composites modernes) possèdent une symétrie à peu près orthotrope. Dans la limite des approximations de la théorie de la courbure des plaques minces, les propriétés vibratoires linéaires de ces feuilles sont gouvernées par quatre constantes élastiques et quatre constantes d'amortissement (pour une fréquence donnée quelconque). Nous présentons une procédure simple qui permet de déterminer, de façon rapide et raisonnablement précise, les quatre constantes élastiques, à partir des modes de basse fréquence de plaques rectangulaires minces à bords libres. On peut aussi déterminer au moins trois des quatre constantes d'amortissement en mesurant les facteurs d'amortissement des mêmes modes (il s'avère que la quatrième constante d'amortissement n'a en général pas assez d'effet sur les modes de basse fréquence pour que l'on trouve une valeur sûre par cette approche). Nous illustrons cette procédure avec des mesures effectuées sur une gamme de différents matériaux lamellaires: plaques de bois découpées sous différents angles dans la poutre d'origine, contre-plaqué et deux composites renforcés par fibres très différents. La discussion de ces résultats expérimentaux suggère que cette procédure simple devrait faire partie de tout programme de contrôle de qualité, de sélection de matériaux ou d'essai non destructif concernant les matériaux lamellaires orthotropes.

**Zusammenfassung**—Viele der bekannten flächenhaften Materialien, von den natürlichen Materialien wie Holz bis zu modernen Verbundmaterialien, weisen näherungsweise orthotrope Symmetrie auf. Die Schwingungseigenschaften solcher Platten sind im Rahmen der Näherungen der Theorie der Biegung dünner Platten durch vier elastische Konstanten und vier Dämpfungskonstanten (bei einer festen Frequenz) bestimmt. Eine einfache Methode wird vorgeschlagen, mit der alle vier elastischen Konstanten rasch und ausreichend genau aus Messungen der Resonanzfrequenzen der niederfrequenten Schwingungsmoden dünner rechteckiger Platten mit freien Kanten bestimmt werden können. Außerdem können mindestens drei der vier Dämpfungskonstanten aus denselben Moden ermittelt werden; es stellt sich heraus, daß die vierte Dämpfungskonstante die Niederfrequenzmoden üblicherweise nicht ausreichend beeinflusst, um mit dieser Methode bestimmt werden zu können. Das Verfahren wird anhand von Messungen an verschiedenen Materialien beschrieben, Holzplatten, die unter verschiedenen Winkeln zum Stamm geschnitten sind, Sperrholz und zwei sehr unterschiedliche faserverstärkte Verbundwerkstoffe. Die Diskussion dieser experimentellen Ergebnisse legt nahe, daß dieses einfache Verfahren eine wertvolle Ergänzung für die Qualitätskontrolle, Materialauswahl oder Materialprüfung darstellt.

## 1. INTRODUCTION

Vibration problems involving orthotropic plates are common, ranging from vibration control in the composite panels of airframe structures or printed-circuit

boards to the design of musical instrument soundboards. In all these problems, one cannot get very far without values for the essential physical parameters of the sheet material in question, in particular the elastic and damping constants for the relevant fre-

quency range. Such values are not readily available in tabulated form, and indeed for many of the materials which we shall be considering there is a wide range of variation between samples of the same nominal material, arising from variations in growth (for natural materials) and in fabrication.

In consequence it is often necessary to measure the elastic and damping constants for the particular plate under study, if vibration predictions of any accuracy are needed. In this paper we describe an approach to making such measurements, based on observing the frequencies and damping factors of low vibration modes of plates with free boundaries, which we believe to be the simplest way to achieve the desired accuracy. Free boundaries offer the only straightforward way to realise in practice a set of boundary conditions which correspond well to theoretical assumptions. The elastic constants can be measured with the absolute minimum of equipment (indeed, with a sufficiently good musical ear they can be determined with no equipment at all). Quantitative determinations of damping constants require a little more apparatus and a great deal more care. The main problem here does not lie in measuring modal damping rates so much as in ensuring that the damping rate observed does indeed arise only from internal damping in the plate, and not from additional losses into the plate's supports or the observer's instrumentation.

For many of the materials relevant to this study, a measurement method based on low-frequency vibration is not only the simplest approach: it is also the *only* approach which does not suffer from grave difficulties of principle when we wish to use the results to make predictions in that same range of frequencies. There are two other general methods which might be used, static measurements [e.g. 1, 2] and ultrasonics [e.g. 3, 4], but neither is wholly appropriate for our purposes. The difficulties are most obvious when it comes to the determination of damping "constants", since these would be expected to be frequency dependent. But even for the measurement of elastic constants there are major problems. With static measurements we must allow for the fact that most relevant materials are at least in part polymeric, of a kind subject to significant levels of creep, so that the results of static tests are hard to relate to vibration problems. The only way is to make model assumptions about microstructure [e.g. 5], whose quantitative accuracy may be dubious. With ultrasonic methods, the main difficulties are two-fold. First, many of the relevant materials are very lossy so that it is hard to obtain strong ultrasonic transmission. Second, many of the materials under study are composites of one kind or another, with some sort of structure on millimetre scales. This can cause significant dispersion of sound waves with wavelengths below a few millimetres, which often turns out to be the order of magnitude of the wavelengths used in conventional ultrasonic testing [8].

For the purposes of this study, an orthotropic plate is one whose elastic behaviour (as described by thin-plate theory) exhibits mirror symmetry with respect to two mutually perpendicular axes in the surface [1, 2]. We are interested in bending vibrations of such plates. Plates meeting this description, to a reasonable approximation, arise in a wide variety of ways. In fact, most familiar sheet materials are of this nature—corrugated sheet, plywood, fibre-reinforced composites and conventionally-cut wooden boards all qualify. An example which will prove quite interesting is the composite material used for printed circuit boards, which contains a rectangular array of reinforcing fibres. Isotropic sheet materials are included as a special case, but in fact many materials usually regarded as isotropic turn out on closer examination to be orthotropic. Sheet metal produced by a rolling process is an obvious example—there will generally be a difference in elastic properties between the directions parallel and perpendicular to the rollers.

Some of the materials listed above can be regarded as sheets cut from a three-dimensional orthotropic solid. It is obvious that a plate cut parallel to one of the symmetry planes of such a solid will have orthotropic symmetry. It is also true, if perhaps slightly less obvious, that a flat plate cut from an orthotropic solid in such a way as to contain *one* of the symmetry axes of the material will be orthotropic in the sense used here. This will be shown in the next section.

This latter case is relevant to the study of wooden plates [1, 2, 6–8]. If the curvature of the annual rings of the tree is neglected, then wood can be regarded as an orthotropic solid. Boards are usually sawn parallel to the axis of the tree, thus containing one symmetry axis of the material (the "grain"). A board cut precisely radially will lie in a symmetry plane, and is described as "quarter-cut". More generally, though, the annual rings will pass through the plate at some angle other than normal, a so-called "slab-cut" board. When wood is selected for musical instrument soundboards, quarter-cut boards are always preferred. However, much of the wood sold even for this purpose is not precisely quarter-cut, and an understanding of the resulting variations in elastic and damping properties, which turn out to be sensitive to ring angle, is very important for quality control.

In this paper we give measured results for five different plates which illustrate the range of possible applications of the approach. Under the general heading of composite plates we consider one of plywood, one of glass fibre reinforced circuit board, and one laminated plate consisting of unidirectional carbon fibres bonded to both sides of a light core material. We also study two plates of Norway spruce (*Picea abies*), one quarter-cut and one not, both sold as being of suitable quality for use in musical instruments.

The outline of the paper is as follows. In the next

section the required elasticity theory is summarised. Also the method of treating small damping by linear viscoelasticity theory is described, following the approach taken in an earlier paper reporting on measurements of isotropic plates [9]. In Section 3 the determination of elastic constants is discussed in detail, and Section 4 does the same for damping constants. In both these sections results for the plywood plate will be used to illustrate the methods.

In Section 5 the measurements for four more plates are given, and the results for all five plates discussed. In each case, some special feature of the construction of the individual plate will show up as a peculiarity of the elastic or damping behaviour revealed by the measurements. This discussion is included not because the particular parameter values measured are of any special significance, but because it illustrates the benefits which accrue from having a simple and straightforward way of carrying out the measurements, and the accompanying insights into material structure. It seems likely that any procedure for material selection or quality control involving orthotropic sheet materials could benefit from incorporating a measurement technique of this kind.

Finally, in Section 6 we discuss the various sources of error which affect the measurements described, with a view to arriving at a realistic idea of the accuracy to be expected. Two general types of error are discussed. First, there are errors due to material imperfections and inhomogeneities of various kinds, which limit the applicability of homogeneous continuum theory to the plate in question. Second, there are errors arising from departures from the thin-plate approximation employed here, which can in principle be allowed for, at some cost to simplicity, if maximum accuracy is needed. Such things as shear corrections, rotatory inertia corrections, edge effects and air loading effects fall under this heading.

## 2. THEORETICAL BACKGROUND

The bending vibrations of a thin, flat, orthotropic plate are governed by four independent elastic constants. The most useful way to define these is through the elastic potential energy. For a plate of small thickness  $h$ , lying initially in the  $xy$  plane and vibrating with a centre-plane transverse displacement  $w(x, y)e^{i\omega t}$ , the relevant "potential energy functional" can be written [1, 2, 6, 9]

$$V = \frac{1}{2} \iint h^3 (D_1 w_{xx}^2 + D_2 w_{xx} w_{yy} + D_3 w_{yy}^2 + D_4 w_{xy}^2) dA \quad (1)$$

where subscripts  $x$  and  $y$  denote partial derivatives, and the double integral is taken over the area of the plate. We shall be mainly concerned with plates of uniform thickness and elastic properties, although the expression (1) remains correct for slow variation of these quantities with  $x$  and  $y$ . The problem of interest is to measure the four elastic constants  $D_1$ ,  $D_2$ ,  $D_3$

and  $D_4$ , and the four associated damping constants.

It might seem odd to work in terms of the foregoing definitions of the elastic constants when more familiar quantities like Young's moduli and shear moduli could be used. However, it is only in certain cases (see below) that we can express the  $D$ s as introduced here in terms of those quantities. For a general thin orthotropic plate, which might for instance have a sandwich structure, the  $D$ s provide the only simple description. Besides, any approach based on variational arguments, including finite-element calculations, will take  $V$  as its starting point and will thus bring in the  $D$ s in any case.

For vibration at angular frequency  $\omega$  the corresponding "kinetic energy functional" is

$$\omega^2 T = \frac{\omega^2}{2} \iint \rho h w^2 dA \quad (2)$$

where  $\rho$  is the volume density of the material. When  $w(x, y)$  is a vibration mode of the plate, Rayleigh's principle gives the corresponding natural frequency  $\omega$  as

$$\omega^2 = V/T \quad (3)$$

(however  $w$  is normalised), with error of order  $\epsilon^2$  if  $w(x, y)$  is known with error  $\epsilon$ .

For the purposes of comparison with other work on this subject, we record the equation of motion of the plate, which may be deduced from equations (1) and (2) by the usual method of the calculus of variations. For a plate of uniform thickness, and uniform  $D_1$  to  $D_4$ , this is

$$\rho \omega^2 w = h^2 [D_1 w_{xxxx} + (D_2 + D_4) w_{xxyy} + D_3 w_{yyyy}]. \quad (4)$$

We consider only rectangular plates cut with sides parallel to the symmetry directions of the material. The boundary conditions appropriate to this equation, for a straight, free boundary  $y = y_0 = \text{constant}$  parallel to the  $x$ -axis, are [6, see Appendix]

$$D_2 w_{xx} + 2D_3 w_{yy} = 0 \quad (5)$$

and

$$2D_3 w_{yyy} + (D_2 + 2D_4) w_{xxy} = 0, \quad (6)$$

both relations to be satisfied at  $y = y_0$ . The boundary conditions on a boundary  $x = x_0 = \text{constant}$  have the same form, with  $x$  and  $y$  and  $D_1$  and  $D_3$  interchanged. An additional condition

$$w_{xy} = 0 \quad (7)$$

must be imposed at right-angled corners where two such boundaries meet. Notice that, while the equation of motion (4) contains only three independent elastic constants (this depends on the spatial uniformity of  $h$ ,  $D_1$ ,  $D_2$ ,  $D_3$  and  $D_4$ ), the fourth constant still enters the problem through the boundary conditions, a point which is sometimes overlooked by workers who have approached this problem via equations of motion rather than energy functions. The

experimental and numerical results to be presented later will confirm that all four elastic constants do indeed influence mode frequencies independently.

Once we know to reasonable accuracy a particular mode shape and its frequency  $\omega$ , it is quite easy to calculate the damping of that mode. It is convenient, and probably at least as accurate as any practical measurement technique, to use a "small damping" approximation which assumes that the modal  $Q$ -factor is much greater than unity. We first introduce the four small quantities  $\eta_1$  to  $\eta_4$ , defined by

$$\eta_i = \text{Im}(D_i)/\text{Re}(D_i), \quad i = 1, 2, 3, 4 \quad (8)$$

(in other words the conventional loss factors associated with the individual complex  $D$ s). The reciprocal of the modal  $Q$ -factor of any given mode can be shown from Rayleigh's principle to be simply a weighted sum of the four  $\eta$ s [9]. The expression is

$$Q^{-1} = \eta_1 J_1 + \eta_2 J_2 + \eta_3 J_3 + \eta_4 J_4 \quad (9)$$

where the  $J$ s are real quantities evaluated from the elastic mode shape,

$$J_1 = \frac{D_1 \iint h^3 w_{xx}^2 dA}{\omega^2 \iint \rho h w^2 dA}, \quad J_2 = \frac{D_2 \iint h^3 w_{xx} w_{yy} dA}{\omega^2 \iint \rho h w^2 dA}$$

$$J_3 = \frac{D_3 \iint h^3 w_{yy}^2 dA}{\omega^2 \iint \rho h w^2 dA}, \quad J_4 = \frac{D_4 \iint h^3 w_{xy}^2 dA}{\omega^2 \iint \rho h w^2 dA}, \quad (10)$$

so that [as can be seen immediately from (1)–(3)]

$$J_1 + J_2 + J_3 + J_4 = 1. \quad (11)$$

The expressions (10) for the  $J$ s simply indicate the partitioning of potential energy, and thus dissipation rate, among the types of motion associated with each of the  $D$ s in equation (1).

The  $J$ s have another significance purely in terms of mode frequencies, which is also worth noting for future reference: it follows, again from Rayleigh's principle, that each  $J_i$  gives the rate of change of mode frequency with the corresponding  $D_i$  according to

$$J_i = \frac{D_i}{\omega^2} \frac{\partial \omega^2}{\partial D_i}, \quad i = 1, 2, 3, 4. \quad (12)$$

This result proves useful when fitting trial values of the  $D$ s to experimental data on  $\omega$ s.

Equations (1)–(12) form the basis both for measurements of the material properties of a flat orthotropic plate, and for applications of the measured values to predict the plate's behaviour. For example, we have used extensions of the theory to study the effects of plate thickness adjustments or changes to the boundary conditions [9]. In that reference we also describe experimental tests confirming the applicability of the basic theory to isotropic plates. The results to be given in Sections 3, 4 and

5 will extend the experimental tests to orthotropic plates.

Before going on to describe the experimental method, it is useful to note the relationship between the elastic constants  $D_1$ ,  $D_2$ ,  $D_3$  and  $D_4$  and the more familiar elastic constants. One thing we can deduce about them which applies to any thin, flat orthotropic plate (with no assumption that it is a slice cut from an orthotropic solid) follows from considering a long, narrow strip cut from the plate. Such a strip will vibrate as a bending beam. If it is cut along a principal axis of the plate it is readily shown that the effective Young's moduli for the beam behaviour are respectively

$$E_x = 12[D_1 - D_2^2/4D_3]$$

or

$$E_y = 12[D_3 - D_2^2/4D_1] \quad (13)$$

for a strip cut along the  $x$  or  $y$  axis. The strip width is taken to be very small compared with the bending wavelength, but still large compared with the plate thickness  $h$ . For such a strip cut from the plate at an angle  $\theta$  to one principal axis (the  $x$ -axis), the equivalent Young's modulus can be shown to be [1, 2, 9]

$$E_\theta = 3D_4(4D_1D_3 - D_2^2)/\Gamma(\theta) \quad (14)$$

where

$$\Gamma(\theta) = D_4(D_1 \sin^4 \theta + D_3 \cos^4 \theta) + (4D_1D_3 - D_2^2 - D_2D_4) \sin^2 \theta \cos^2 \theta.$$

Note from this last expression that  $\sin \theta$  and  $\cos \theta$  enter only in the three combinations  $\sin^4 \theta$ ,  $\cos^4 \theta$  and  $\sin^2 \theta \cos^2 \theta$ . It follows that, as was pointed out in Ref. [9], only three independent combinations of the (complex) constants  $D_1$  to  $D_4$  can be deduced from frequency and damping measurements on strips cut from a thin plate (for example, we might measure  $E_x$ ,  $E_y$  and  $E_\theta$  for  $\theta = \pi/4$ ). This fact is worth noting, since measurements on strips, based on bending-beam theory, have been extensively used in the past for determining Young's moduli [10–12]. We should not be too surprised that strips cannot be used to determine all four of the plate constants: it is well known for isotropic plates that only Young's modulus, and not Poisson's ratio, can be deduced from frequency measurements on strips [e.g. 9]. This fact suggests the use of plates rather than strips, which is the main subject of this paper.

If our flat plate is cut from an orthotropic solid, then the four constants  $D_1$  to  $D_4$  which we have used can be related to the Young's moduli along the two principal directions  $E_x$  and  $E_y$  [equation (13) above], the two Poisson's ratios between the  $x$  and  $y$  directions  $\nu_{xy}$  and  $\nu_{yx}$ , and the in-plane shear modulus  $G_{xy}$ . The notation  $\nu_{xy}$  refers to the Poisson contraction in the  $y$  direction when a stretch is applied in the  $x$  direction, while  $\nu_{yx}$  refers to the converse situation. The simplest case occurs when the plate is cut from

the solid parallel to one of the principal planes. In that case, values for the four  $D$ s can be obtained from equations (7.3.2) of Hearmon [2]

$$\begin{aligned} D_1 &= E_x/12\mu, & D_2 &= v_{xy}E_y/6\mu = v_{yx}E_x/6\mu \\ D_3 &= E_y/12\mu, & D_4 &= G_{xy}/3 \end{aligned} \quad (15)$$

where  $\mu = 1 - v_{xy}v_{yx}$ .

There is a simple reciprocal property relating the two Young's moduli and the two corresponding Poisson's ratios, so that only three of these are independent, a fact used in exhibiting the symmetrical property of  $D_2$  in (15) above

$$v_{yx}/E_y = v_{xy}/E_x. \quad (16)$$

This follows from a general reciprocal theorem discussed by Rayleigh [13, Section 107]. The fourth independent constant is the shear modulus  $G_{xy} = 3D_4$ , which refers to *in-plate* shear, i.e. to the kind of shear in which a small square element on the top or bottom surface of the plate is deformed into a parallelogram. This is exactly what occurs in a pure twisting motion such as  $w = xy$ , which thus excites only the  $D_4$  term in the potential energy function, equation (1).

It is a useful check to notice that if the expressions (15) are substituted into the left-hand sides of equations (13), the right-hand sides  $E_x$  and  $E_y$  are indeed recovered. Another useful check is the version of equation (15) applicable to an *isotropic* plate: we have

$$\begin{aligned} D_1 &= D_3 = E/12(1 - \nu^2) \\ D_2 &= \nu E/6(1 - \nu^2) \\ D_4 &= E/6(1 + \nu) \end{aligned} \quad (17)$$

in terms of Young's modulus  $E$  and Poisson's ratio  $\nu$ . Substituting these values into equation (14) recovers  $E$  and into (1) recovers the familiar potential energy function of a thin plate cut from an isotropic solid [e.g. 13, Section 214].

Finally, we give expressions for the  $D$ s for a flat plate cut from an orthotropic solid in a plane containing only one of the symmetry axes of the material. Our account is based on Hearmon's, which is given most clearly for our purposes in Ref. [1], p. 26, although the more readily obtainable Ref. [2], Section 1.5 covers the same material in more general terms. For definiteness, we give the discussion in terms of the application to wood. The three principal directions in the tree are conventionally denoted R (radial), T (tangential) and L (longitudinal). We discuss explicitly the important case of "ring tilt", for which the L-axis lies in the plate but neither the R nor T axis does. This contrasts with the ideal "quarter-cut" plate, which lies in the RL plane with the annual rings running through the plate normal to its surface.

The starting point for analysis is the  $6 \times 6$  compliance matrix  $S_{ij}$ , which transforms the six stress components  $\sigma_1, \dots, \sigma_6$  into the six strain components  $e_1, \dots, e_6$  according to the standard formulae [1, 2]

$$e_i = \sum_{j=1}^6 S_{ij} \sigma_j$$

where  $e_1, e_2, e_3$  ( $=e_R, e_T, e_L$ ) are the three direct strain components and  $e_4, e_5, e_6$  ( $=e_{TL}, e_{LR}, e_{RT}$ ) the three shear strain components, with a similar notation for the stresses  $\sigma_j$ . If principal axes are taken, then  $S_{11}, S_{22}, S_{33}$  are the reciprocals  $1/E_1, 1/E_2, 1/E_3$  ( $=1/E_R, 1/E_T, 1/E_L$ ) of the corresponding Young's moduli,  $S_{44}, S_{55}, S_{66}$  are the reciprocals of the TL, LR, RT shear moduli, and  $S_{12} = S_{21} = -v_{RT}/E_R = -v_{TR}/E_T$  with two similar formulae for  $S_{23}, S_{31}$ . If we take axes rotated through an angle  $\theta$  about the L axis, then from standard tensor theory

$$\begin{aligned} S'_{11} &= S_{11}m^4 + (2S_{21} + S_{66})m^2n^2 + S_{22}n^4 \\ S'_{13} &= S'_{31} = S_{13}m^2 + S_{23}n^2 \\ S'_{33} &= S_{33} \\ S'_{55} &= S_{55}m^2 + S_{44}n^2 \\ S'_{15} &= S'_{51} = S'_{35} = S'_{53} = 0, \end{aligned} \quad (18)$$

where primes denote values in the rotated axes, and  $m = \cos \theta$ ,  $n = \sin \theta$  [1, equation (10), 2, Section 1.5].

The essential approximation of thin plate theory is that the deformed plate is in a state of plane stress, in which the three stress components acting in the plane are much larger than the other three, cross-plane, stresses [e.g. 14]. It is thus a justifiable approximation to delete from the compliance matrix the columns applying to the three cross-plane stress components, and the rows corresponding to the three cross-plane strain components, in which we are not interested, leaving a (symmetric)  $3 \times 3$  matrix. The inverse of this  $3 \times 3$  matrix gives the plate stiffnesses which enter into the expression for the potential energy of bending, equation (1) in our case, according to (with  $D_1$  along-grain and  $D_3$  cross-grain)

$$\begin{bmatrix} 12D_3 & 6D_2 & 0 \\ 6D_2 & 12D_1 & 0 \\ 0 & 0 & 3D_4 \end{bmatrix} = \begin{bmatrix} S'_{11} & S'_{13} & 0 \\ S'_{31} & S'_{33} & 0 \\ 0 & 0 & S'_{55} \end{bmatrix}^{-1} \quad (19)$$

in which  $\theta = 0$  corresponds to the quarter-cut plate, lying in the 13 or RL plane. For a flat plate cut at a completely general angle to the principal axes, the rotation formulae are more complicated than equations (18) and the  $3 \times 3$  matrix has no zero elements. We would then need *six* independent elastic constants to describe the plate vibrations, the four-constant theory discussed in this paper would not be relevant, and the plate would not behave orthotropically with respect to bending motions.

Performing the matrix inversion of equation (19) and substituting from equations (18) now yields the formulae

$$D_1 = \frac{1}{12\Delta} \left\{ \frac{m^4}{E_R} + \left( \frac{1}{G_{RT}} - \frac{2v_{RT}}{E_R} \right) m^2 n^2 + \frac{n^4}{E_T} \right\} \quad (20)$$

$$D_2 = \frac{1}{6\Delta E_L} \{ v_{LR} m^2 + v_{LT} n^2 \} \quad (21)$$

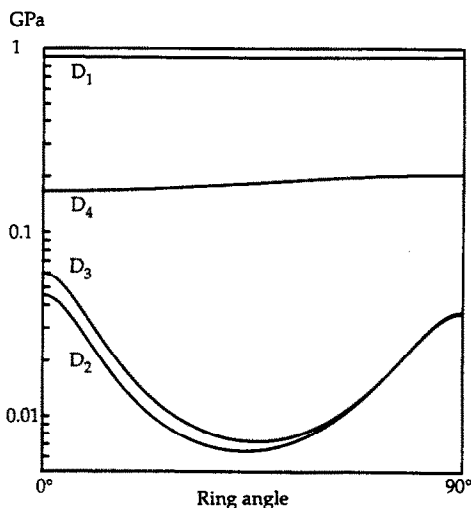


Fig. 1. The four elastic constants  $D_1$  to  $D_4$  for a flat plate of spruce, calculated according to equations (20)–(24) using the data from Ref. [1] reproduced below. The L (longitudinal) symmetry axis of the material (i.e. the “grain”) lies in the plate, and the constants are plotted as a function of angle  $\theta$  of rotation in the RT plane about that axis. This is the angle of the annual rings, and varies linearly from zero (the ideal quarter-cut plate) to  $90^\circ$  (plate in the LT plane). The vertical scale is logarithmic, to allow for the large range of values. The values of the elastic constants used are as follows:  $E_L = 10.7$  GPa,  $E_R = 0.71$  GPa,  $E_T = 0.43$  GPa,  $\nu_{RT} = 0.51$ ,  $\nu_{LT} = 0.51$ ,  $\nu_{LR} = 0.38$ ,  $G_{RT} = 0.023$  GPa,  $G_{LT} = 0.62$  GPa,  $G_{LR} = 0.50$  GPa.

$$D_3 = \frac{1}{12\Delta E_L} \quad (22)$$

$$D_4 = \frac{G_{LR} G_{LT}}{3[m^2 G_{LT} + n^2 G_{LR}]} \quad (23)$$

where  $\Delta = S'_{11}S'_{33} - S'^2_{13}$ , i.e.

$$\Delta = \frac{(1 - \nu_{RL}\nu_{LR})m^4}{E_R E_L} + \frac{(1 - \nu_{LT}\nu_{TL})n^4}{E_T E_L} + \left\{ \left( \frac{1}{G_{RT}} - \frac{2\nu_{RT}}{E_R} \right) \frac{1}{E_L} - \frac{2\nu_{RL}\nu_{LT}}{E_R E_L} \right\} m^2 n^2. \quad (24)$$

[Recall that  $\nu_{RT}/E_R = \nu_{TR}/E_T$ , etc. from equation (16).] Notice that setting  $m = 1$ ,  $n = 0$  recovers equations (15) above for the case of a plate cut in one of the principal planes of the material.

We illustrate these results in Fig. 1. The four constants  $D_1$  to  $D_4$  have been calculated from the above equations, using measured values for the Young's moduli, shear moduli and Poisson's ratios taken from Table 2 of Hearmon [1]. We have used what appears to be a typical set of “spruce” values from that table (values given in the figure caption), since in Section 5 we shall present some measurements of the four  $D$ s for two spruce plates cut at different angles, with which these numbers can be compared. Hearmon lists all six Poisson's ratios, and the measured results do not exactly satisfy the recip-

rocal relations [16]. We have used the larger of each pair of Poisson's ratios in the calculations, since the larger values are less prone to experimental errors [1]. The figure shows all four  $D$ s plotted as a function of ring angle  $\theta$ , on a logarithmic vertical scale since the range of values is so large.

Notice the extreme sensitivity of  $D_2$  and  $D_3$  to ring angle, for this particular wood, revealed by this graph—this is presumably one reason why instrument makers pay such careful attention to ring angle when selecting spruce for soundboards. The main reason for the large variation of  $D_2$  and  $D_3$  is a very small value of  $G_{RT}$  for spruce: this makes  $\Delta$  in equation (24) very large for ring angles in mid-range. For a rod cut in the TR plane at about  $45^\circ$  to the rings, it is easy to visualise large shearing motions between the rings reducing the effective Young's modulus. Schelleng [11] cites A. H. Benade as having made this point.

### 3. MEASURING THE ELASTIC CONSTANTS

The first few vibration modes of a free-edged, rectangular orthotropic plate are illustrated in Fig. 2. The sequence and precise details of mode shapes will depend on the particular values of elastic constants

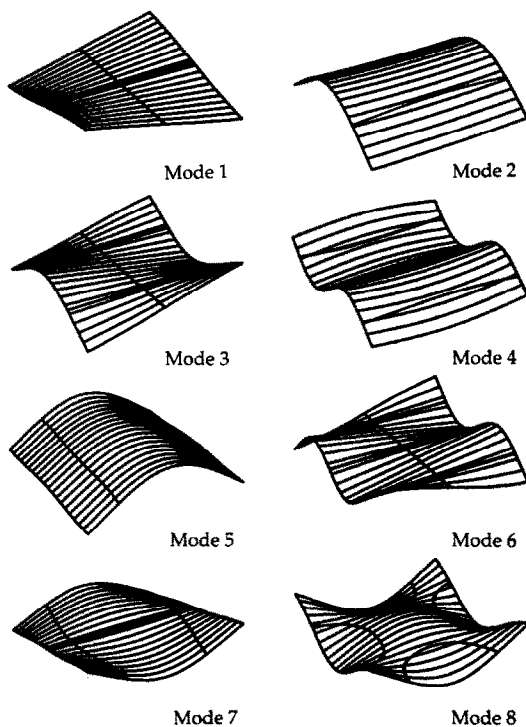


Fig. 2. The first eight vibration modes of a square, free-edged orthotropic plate, with a particular set of values of the elastic constants. The values chosen correspond to plate 3 of this study, as given in Table 5. (Note that mode 6 of this series was not measured on the actual plate, and so is absent from the results in Table 7.) The nodal lines of the modes are shown.

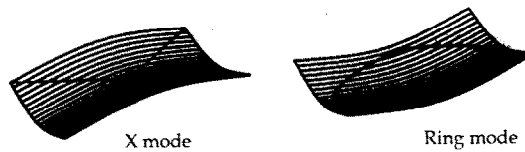


Fig. 3. The X mode and ring mode for a plate of critical aspect ratio [satisfying equation (28)], with the same elastic constants as were used to compute Fig. 2.

and geometrical dimensions, but most plates will exhibit a set of modes clearly identifiable with these pictures, in some order. The only significant exception to this is one which will play a part in the measurement procedure to be described. If the length-to-breadth aspect ratio of the plate is adjusted to a certain special value (to be discussed shortly), the two lowest "bending beam" modes (modes 2 and 5 in Fig. 2) would, in the absence of Poisson's ratio coupling, become degenerate. With such coupling, they combine into two different-looking modes which are approximately the sum and difference of the shapes illustrated in Fig. 2, having frequencies which differ by an amount which is a measure of the strength of the Poisson's ratio coupling [9, 13]. These two modes are illustrated in Fig. 3—for obvious reasons, we shall refer to them as the X-mode and the ring mode.

The aim of this section is to describe an efficient way of deducing values of the four elastic constants  $D_1$ ,  $D_2$ ,  $D_3$  and  $D_4$  from observations of the resonant frequencies of modes like those illustrated in Figs 2 and 3. It will turn out that one can obtain useful first approximations to all four constants without any need for numerical computation. However, for the most accurate answers computations are required. A computer program which serves this purpose with minimal programming effort (provided that a library routine for calculating matrix eigenvectors and eigenvalues is available) is described in the Appendix. All computations in this article have been carried out by the method described there. The computer program has been checked against earlier results obtained by independent methods [9], and against known analytic results for special cases.

The most rapid, reliable and accurate way of measuring mode frequencies for the present purpose is to use the time-honoured method of Chladni patterns. A loudspeaker is mounted beneath a sufficiently large flat surface, and the plate is supported over it on the softest and smallest feasible blocks of foam. These blocks are adjusted to lie accurately under nodal lines of the mode under observation. The loudspeaker is driven by a sine-wave generator, and the frequency is adjusted until the plate resonates in the desired mode, as revealed by a suitable powder sprinkled on the surface. Having tuned to the peak response as carefully as possible, the frequency is determined from a standard counter. Accuracies of 1% or so can usually be achieved quite

easily by this method (but see the detailed discussion of errors and accuracy to be given in Section 6).

The main advantages of this method are (1) one can be sure which mode corresponds to which measured frequency (unlike a method based solely on response-function peaks, where identification of which mode corresponds to which peak is harder); (2) the free boundary conditions assumed by the theory are realised quite accurately since, provided the foam blocks are carefully adjusted, the plate vibration is essentially unconstrained by the method of support; and (3) no transducer is attached to the plate, which might perturb the results by adding mass. It is also very quick to carry out the measurement for the first few modes of a given plate. The process can often be speeded up by tuning the oscillator to roughly the right frequency for each mode, based on tapping the plate and listening. With practice, the frequencies of most of the modes plotted in Figs 2 or 3 (as appropriate) can be elicited by holding the plate at a node of the required mode, tapping at an antinode (perhaps on a node line of other, unwanted, modes), and listening very close to the tapping point. (Such plate-tapping has been used by musical instrument makers since time immemorial when adjusting soundboard thicknesses.)

The first stage of the measurement procedure is to cut an accurately rectangular plate from the sheet material under study, with proportions such that it produces modes like Fig. 2, not Fig. 3. It is most convenient to use a plate which is not too far from square at this stage. Indeed, if the material has significantly different bending stiffnesses in the two principal directions, a square plate is usually very suitable. The plate is measured and weighed, and the lowest few mode frequencies are determined by the Chladni pattern method just described. If damping constants are to be determined, modal  $Q$ -factors should also be measured at this stage; a discussion of that part of the procedure will be given in the next section.

From these measured frequencies, we can immediately obtain first estimates of  $D_1$ ,  $D_3$  and  $D_4$ . Three of the low modes, numbers 1, 2 and 5 in Fig. 2, are particularly simple, such that the frequency of each is determined almost entirely by just one of these three constants (as will be confirmed by the  $J$  values in Tables 3, 6–9 below). We can make simple variational estimates of those three frequencies to obtain formulae for the three constants, to a first

approximation. Mode 1 is more or less pure twisting motion, which is quite well approximated by the function  $w = xy$ . Using this as a trial function (as was done by Rayleigh [13]), we obtain by substitution into (3)

$$D_4 \approx 0.274 f_1^2 \rho a^2 b^2 / h^2 \quad (25)$$

where the plate dimensions are  $a \times b$ , and  $f_1$  is the frequency (in Hz) of the mode corresponding to mode 1 in Fig. 2—it will not necessarily be the lowest mode for every plate, although it usually is.

In a similar way, modes 2 and 5 in Fig. 2 are essentially one-dimensional bending-beam modes. We can thus obtain frequency estimates by using as trial functions free-free beam functions in the  $x$  and  $y$  directions respectively, giving

$$D_1 \approx 0.0789 f_2^2 \rho a^4 / h^2 \quad (26)$$

and

$$D_3 \approx 0.0789 f_5^2 \rho b^4 / h^2 \quad (27)$$

where  $f_2$  and  $f_5$  are the mode frequencies of the lower and higher of the two bending beam modes respectively, corresponding to modes 2 and 5 in Fig. 2. It is of course somewhat arbitrary which direction we associate with  $D_1$  and which with  $D_3$ . For definiteness, the discussion throughout this paper will assume that the choice is made so that  $D_1 \geq D_3$ . For a square plate, this will mean that  $f_2$  is governed principally by  $D_3$  and  $f_5$  by  $D_1$ , as implied by equations (26) and (27). Again, we emphasise that the mode numbering is somewhat arbitrary,  $f_2$  and  $f_5$  being the second and fifth gravest frequencies only for certain ranges of  $D$  values.

Having obtained first estimates of  $D_1$ ,  $D_3$  and  $D_4$  from equations (25) to (27), we can proceed to the second stage of the measurement procedure. To determine  $D_2$ , we achieve maximum accuracy by adjusting the aspect ratio of the plate so as to produce the ring and X modes as in Fig. 3. As already mentioned, these two modes differ in frequency only because of a Poisson's ratio coupling effect. As is shown most clearly by equation (15) for the special case of a plate cut in a principal plane of an orthotropic solid,  $D_2/D_1$  and  $D_2/D_3$  embody this Poisson's ratio effect, so that it is not surprising that the frequency ratio of ring mode to X mode is particularly sensitive to the relative value of  $D_2$ .

The required aspect ratio is given by

$$a/b = (D_1/D_3)^{1/4}. \quad (28)$$

This can be seen by making the change of variables  $\xi = xD_1^{-1/4}$ ,  $\eta = yD_3^{-1/4}$  in the potential energy expression (1). That expression then remains the same if  $\xi$  and  $\eta$  are interchanged, and this is precisely the symmetry possessed by the ring and X modes. We can use the initial estimates of  $D_1$  and  $D_3$  to determine an approximate value of  $a/b$  via equation (28). Fine tuning of  $a/b$  can then be carried out, aided of course by the Chladni patterns. The mode shapes will be

found to be very sensitive to small changes in aspect ratio. Having obtained the two modes, we record their frequencies, and perhaps their modal  $Q$ -factors as further input to the subsequent determination of damping constants.

An approximate value of  $D_2$  can now be obtained by reference to Fig. 4. This contour plot shows the ring-mode-to-X-mode frequency ratio  $f_0/f_X$  as a function of  $D_1/D_3$  (logarithmically along the  $x$ -axis) and  $D_2/D_3$  (linearly along the  $y$ -axis). This figure was computed using the program to be described below and in the Appendix—it is more accurate than the approximate formulae (26) and (27). The  $x$ -axis is also annotated in terms of aspect ratio  $a/b$  (along the top). (Note that in practice the two values of abscissa might not quite agree—see the discussion of errors in Section 6.) For the appropriate value of  $D_1/D_3$ , the ratio  $D_2/D_3$  is read from the  $y$ -axis by finding the contour line corresponding to the observed frequency ratio  $f_0/f_X$ .

As an aside, one can also give approximate formulae for the ring and X mode frequencies which agree well with the function plotted in Fig. 4. Using as trial function an arbitrary linear combination of the free-free beam functions in the  $x$  and  $y$  directions, minimising the Rayleigh quotient in the usual way to determine the coefficients of this linear combination, and finally making small corrections to give a good average fit to the computed contour map over the parameter range plotted in Fig. 4, gives

$$\left. \begin{matrix} f_0^2 \\ f_X^2 \end{matrix} \right\} \approx \frac{h^2}{\rho a^2 b^2} [13(D_1 D_3)^{1/2} \pm 4.4 D_2] \quad (29)$$

assuming that equation (28) is satisfied. To this level of approximation,  $f_0$  and  $f_X$  exhibit no  $D_4$  dependence. The values of  $J_4$  to be given later will confirm this insensitivity. Advantage was taken of this in computing Fig. 4: in principle, one might have needed a whole family of such plots for different values of  $D_4$ , but in fact it proves entirely adequate to give  $D_4$  the *ad hoc* value  $(D_1 D_3)^{1/2}$ , which has roughly the right order of magnitude for realistic plates.

As a corollary, we note in passing a useful pair of formulae for the special case of an *isotropic* plate. For that case, the ring and X modes are obviously produced when the plate is square. From the frequencies of those two modes of a square plate, both Young's modulus and Poisson's ratio can immediately be obtained, approximately, by manipulating equations (17) and (29) to give

$$v \approx 1.48 \left[ \frac{f_0^2 - f_X^2}{f_0^2 + f_X^2} \right] \quad (30)$$

and

$$E \approx 0.46(1 - v^2)(f_0^2 + f_X^2)\rho a^4/h^2. \quad (31)$$

The final stage of the procedure for determining elastic constants involves improving the first estimates which we now have, with the aid of a computer program for determining plate frequencies more



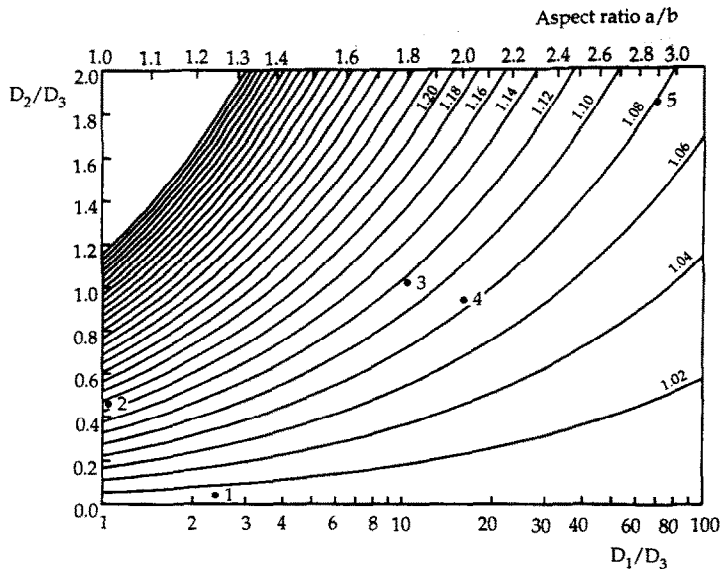


Fig. 4. Contour map of the ratio of ring mode frequency  $f_0$  to X mode frequency  $f_x$  of a rectangular, orthotropic plate, encompassing the range of elastic constants likely to be encountered in practice. In computing this figure, the length-to-breadth aspect ratio of the plate was always scaled to satisfy equation (28). Although it makes little difference to the results,  $D_4$  was always set to  $\sqrt{(D_1 D_3)}$ , to give it a broadly realistic value. The contours of equal frequency ratio are labelled where space permits, and continue with the same spacing thereafter. The points labelled 1–5 correspond to the five plates measured in this study. Notice the wide range of parameters thus represented.

accurately than the estimates given above. A simple program to do that job, which works entirely adequately for the purpose in hand, is described in the Appendix. It is based on a variational method with power-series trial functions. While certainly not optimal from a numerical analysis standpoint, this approach makes the programming, including the calculation of auxiliary functions such as the  $J$ s [equations (10)], very easy.

This final stage is best described by working through an example, so we now give some measured data for a real plate. The plate we have chosen to illustrate the method is of commercial birch 5-ply, with a mean thickness of 6.36 mm and a density of 673.6 kg/m<sup>3</sup>. In accordance with the procedure just described, measurements were made on a square plate, 225 × 225 mm. The measured frequencies for the first eight modes are shown alongside sketches of the mode shapes in the first columns of Table 1. (Note that the order of the modes is indeed different from that in Fig. 2.) The final two rows of that table show the X mode and ring mode frequencies, obtained in this case while the plate was bigger, at 280 × 225 mm. Applying equations (25)–(27) with these data yielded first estimates of  $D_1$ ,  $D_3$  and  $D_4$  as shown in the first row of Table 2. The figure for  $D_2$  in that same row was obtained from the ring and X mode frequencies as described above—the appropriate point is marked on Fig. 4 and labelled 1.

We now take these first estimates for the  $D$ s, and run the program to predict the corresponding plate frequencies. The results are shown in the third

Table 1. Measured and predicted mode frequencies (all in Hz) for the plywood plate, as described in the text

Mode	Measured	First estimates	Predictions		
			A	B	C
1		138	135	138	138
2		356	356	356	349
3		440	448	452	444
4		541	541	541	541
5		611	604	607	607
6		819	850	857	853
7		955	981	981	955
8		1040	1060	1063	1039
		349	355	355	347
		352	358	358	350

The ring and X mode frequencies shown here were calculated in each case using an aspect ratio satisfying equation (28). The diagrams of mode shapes are schematic only, and do not reproduce the plate proportions or the details of the true mode shapes.

Table 2. Estimated values of the four elastic constants  $D_1$ ,  $D_2$ ,  $D_3$  and  $D_4$  for the plywood plates, corresponding to the predicted frequencies shown in the respective columns of Table 1, as described in the text

	$D_1$	$D_2$	$D_3$	$D_4$ (MPa)
First estimate	986	15	427	223
Refined, A	986	15	427	233
Refined, B	986	15	404	233
Refined, C	986	15	411	233

column of Table 1, headed “First estimates”. Quite good agreement with the observed frequencies is revealed, but the disagreements suggest that there is some scope for fine tuning to improve the fit. One way to proceed is to look again at the same three modes which were used in the initial formulae, equations (25)–(27). In this case, these are modes 1, 2 and 4. If these frequencies do not agree, it is easy to adjust the values of the  $D$ s so that they do, in a manner to be indicated shortly. This particular example is somewhat unusual in that the two bending beam modes, 2 and 4, agree exactly already. This is a consequence of the very small value of  $D_2$  for this plate—the approximate formulae (26) and (27) become exact when Poisson’s ratio effects are absent, as Rayleigh has described [13, Section 226]. This very small value of  $D_2$  has an interesting physical interpretation, which will be explained near the end of Section 5.1 when we have data from other plates with which to contrast it.

To improve the match of these simple modes, we make use of equation (12) and the computed values of the  $J$ s, given for this plate in Table 3. Notice that the pattern of  $J$ s for the three modes in question is especially simple—in each case, one  $J$  is approximately equal to unity, and all the others are approximately zero. Thus to improve the fit of mode 1, for example, we change  $D_4$  (since  $J_4 \simeq 1$  is the non-zero entry for that mode) according to equation (12) (with  $\omega = 2\pi f$ ). Equivalently, the new  $D_4$  is given by the old  $D_4$  multiplied by the square of the ratio of the observed frequency to the first predicted frequency, i.e. by  $(138/135)^2$  in this case. Having corrected  $D_4$  in this way, and  $D_1$  and  $D_3$  similarly, according to the three simplest modes,  $D_2$  is revised if need be by reference to Fig. 4 and the program is run again. In principle this procedure should be iterated, but in practice it will usually be found to give adequate accuracy after one iteration.

For the plate under study, this procedure gives the values of  $D$ s and frequencies labelled “A” in both Tables 1 and 2. For most purposes this would be adequate—indeed for many purposes the initial estimates of the  $D$ s might suffice. However, to show some other possibilities and to give an indication of the accuracy of the estimated  $D$ s, and the limitations of the theory, we give also two other examples of slightly different choices of adjusted  $D$  values. Notice from Table 1 that although we have matched the lowest bending beam modes well, the second bending beam mode in one direction, mode 7 in Table 1, is not

well predicted. The ratio of the two bending beam frequencies 2 and 7 will be influenced hardly at all by values of the  $D$ s, since it is fixed by beam theory, so the fact that this ratio is wrong here is an indication either of departures from ideal thin-plate behaviour or of material inhomogeneity, and thus of the limits on achievable accuracy in predictions of the  $D$ s. To illustrate this, in the predictions labelled “B” in Tables 1 and 2,  $D_3$  has been adjusted so that mode 7 rather than mode 2 is matched (note that mode 7 also has  $J_3 \simeq 1$ , so that it too is influenced mainly by  $D_3$ ).

Presumably the “best” value of  $D_3$  would be some compromise between the two used so far, perhaps weighted towards the graver mode since thin-plate theory should be better for that mode, and the effects of material inhomogeneity perhaps less. One independent indication of a suitable value comes from the aspect ratio needed to tune the plate to produce the ring and X modes. This should come close to satisfying equation (28). [Note that the frequencies listed in Table 1 for the ring and X modes for cases A and B were calculated with a value of  $a/b$  satisfying equation (28), which differed slightly from the actual value.] With this in mind, we give results for the same value of  $D_1$  as before, but with the value of  $D_3$  adjusted to  $D_1 \times (225/280)^4$ , in the case labelled “C” in Tables 1 and 2. Here, nearly all frequencies are well matched, the main exceptions being modes 2, 6 and 7. Perhaps this does indeed represent the “best” set of  $D$ s for this particular plate. But notice that mode 6 is consistently over-predicted, suggesting that some of the higher modes of this particular plate do not satisfy thin-plate theory to very high accuracy. Certainly this plate is quite thick, and the ratio of frequencies of modes 2 and 7 departs from that predicted by thin-plate theory in the right direction for the first effects of thick-plate corrections. Another possible reason for the deviations from predicted frequencies is simply inhomogeneity of the material properties. The individual veneers from which plywood is made may vary quite significantly from point to point, and although there will be some averaging-out of these fluctuations from the contributions of the different layers, some of the inhomogeneity would be expected to survive in the bending properties of the finished sheet. Sources of error will be discussed in more detail in Section 6.

4. MEASURING THE DAMPING CONSTANTS

To determine the damping constants  $\eta_1, \eta_2, \eta_3$  and  $\eta_4$  requires simpler theory but trickier measurements than were used in the previous section to determine elastic constants. Once we have computed mode shapes, it is very easy to calculate the dimensionless factors  $J_1, J_2, J_3$  and  $J_4$  for each mode. Given measured values of the modal  $Q$ -factors, we have in principle only to solve a linear problem to infer the

$\eta$ s from equation (9). In practice, however, equation (9) will not be exactly satisfied—experimental errors will ensure this, even if the underlying theory is accurate. However, a simple linear regression method can be used to find the set of  $\eta$ s which give the best least-squares fit of predictions from equation (9) to a set of measured  $Q$ s.

Unfortunately, the accurate experimental determination of modal  $Q$ -factors is by no means easy. The main problem is to support a “free” plate without adding significant damping; foam blocks are of no use here. The method we have used involves locating the nodal lines of the modes under consideration by the Chladni pattern technique, then drilling a very small hole in the plate somewhere on each node line. By choosing intersections of node lines of different modes, the number of holes drilled can be minimised. (One hole in the centre copes with the majority of modes.) For a given mode, the plate is then suspended by a fine nylon thread passed through the appropriate hole. Since there will be no motion at the suspension point from the mode in question, the thread will cause no energy loss or constraint of the motion. It can be shown theoretically that small holes do not have a significant effect on the potential energy of the plate, and it has also been confirmed experimentally that the measured  $Q$ s are not influenced by the number of holes drilled.

A very small accelerometer is then attached to the plate, close to a node line. Here a compromise must be struck. It must be far enough from the node line to give some reading, but as close as possible so that the mass and damping of the accelerometer and its lightweight cable do not influence the behaviour

unduly. The plate having thus been supported and instrumented, the response to an impulsive drive is digitised into a small computer via a 12-bit analogue-to-digital converter. For the low frequencies under consideration here, a tap with a rubber-ended pencil is a suitable excitation. The virtue of impulsive excitation is that there is no exciter in contact with the plate during the free decay period, which is the portion of the signal which we analyse to determine the  $Q$ -factor. One could perhaps achieve some useful improvement in accuracy by replacing the accelerometer with an optical sensor of some kind, but we have not explored this possibility.

The temporal decay rate of the mode in question is calculated by a computer program which takes a series of short FFTs, stepping on a few time points each time. Peaks are found, and best-fitting exponential decays calculated on the basis of the variation of the peak height with time. A measure of the quality of fit is also displayed on the screen, so that bad data can be excluded from the measurements. By analysing in this way a number of takes for each mode—say 20—an average decay rate can be calculated, and turned into a  $Q$ -value using the accurately-known frequency from the measurements described in the previous section. (It is important not to use the frequency obtained from the short FFTs of the decay rate calculation, since these take only a very short time window and thus do not have sufficient frequency resolution.) By this method,  $Q$ -values accurate to perhaps 2% (for the range of values of interest here) can be obtained if sufficient care is taken.

Results of such measurements for the plywood plate studied in the previous section are shown in the first two columns of Table 3.  $Q$ -values are given for

Table 3. Measured and calculated modal  $Q$ -factors for the plywood plate, as described in the text, together with the dimensionless factors  $J_1$ ,  $J_2$ ,  $J_3$  and  $J_4$  calculated using the elastic constants from the final row of Table 2

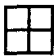







Mode		Measured $Q$	First predicted $Q$	Final predicted $Q$	$J_1$	$J_2$	$J_3$	$J_4$
1		43	43	43	0.013	0.000	0.023	0.965
2		83	83	78	0.000	−0.000	1.000	0.000
3		59	61	59	0.012	0.001	0.618	0.370
4		91	91	95	1.000	0.000	0.000	0.000
5		82	74	76	0.796	0.001	0.009	0.194
6		58	61	61	0.410	0.003	0.182	0.406
7		75	83	78	0.000	−0.000	1.000	0.000
8		67	73	69	0.006	0.001	0.848	0.145

Table 4. Estimated loss factors  $\eta_1$ ,  $\eta_3$  and  $\eta_4$  for the plywood plate

	$\eta_1$	$\eta_3$	$\eta_4$
First estimate	0.0110	0.0120	0.0237
Final estimate	0.0105	0.0128	0.0239

all the modes of the plate when square, but for this particular plate it proved impossible to obtain reliable  $Q$ s for the ring and X modes by this method, since the two frequencies were within a damping bandwidth of each other. Table 3 also gives the values of  $J_1$ ,  $J_2$ ,  $J_3$  and  $J_4$  for each mode, calculated using the final estimates of the elastic constants, case C in Table 2.

Just as we were able, in the previous section, to obtain useful first approximations to the  $D$ s without computation, so here we can obtain useful estimates of three of the four  $\eta$ s very easily. As we have already noted, the three special modes used before (1, 2 and 4 in this case) each have one  $J$  roughly (here almost exactly) equal to unity and the other three roughly zero. Thus we can estimate  $\eta_1$  simply by  $1/Q$  for mode 4,  $\eta_3$  by  $1/Q$  for mode 2 and  $\eta_4$  by  $1/Q$  for mode 1. We can assess the accuracy of these estimates by evaluating the other modal  $Q$ s from equation (9) and the computed  $J$ s, taking  $\eta_2 J_2$  provisionally equal to zero. The result is shown in column three of Table 3, headed, "First predicted  $Q$ ", and the values of  $\eta_1$ ,  $\eta_3$  and  $\eta_4$  used are given in Table 4. A reasonable correspondence with the measured  $Q$ s is obtained for all modes.

To get the best estimates of the  $\eta$ s, however, we want to use equation (9) and all the measurements in an attempt to average out experimental errors. This is a standard linear regression problem, to calculate the values of the  $\eta$ s which minimise the sum of squares of deviations of predictions from observations. At this stage we might think of bringing  $\eta_2$  into the picture as well, but for this particular plate a glance at the values of  $J_2$  shows that this would be pointless. Because of the remarkably small value of  $D_2$  for this plate, all the values of  $J_2$  are so small as

to be irrelevant. Physically, the in-plate Poisson contraction is so weak that the corresponding damping contribution is *prima facie* unlikely to be brought into play by any plate vibration mode. Any influence of  $\eta_2$  on  $Q$ -factors would be lost in the experimental noise. Thus we carry out the regression process on  $\eta_1$ ,  $\eta_3$  and  $\eta_4$  only, obtaining the best-fitting values listed in Table 4 and the best predicted  $Q$ s given in column four of Table 3. The general level of agreement is now remarkably good—if anything better than the agreement between measured and computed frequencies.

When we come to look at other plates, we will find that in some cases we are able to get an estimate of sorts for the value of  $\eta_2$ , while other cases resemble this one in giving no information which is significant to the level of accuracy considered. Thus in conclusion we can say that the methods outlined in this section and the last allow all four elastic constants and three of the four damping constants to be determined with reasonable ease and accuracy. The fourth damping constant can sometimes be estimated, but sometimes has so little influence on the damping of low modes of free plates that it cannot be determined this way. Its value is, of course, of correspondingly limited interest as far as plate bending vibration is concerned.

5. THE REMAINING MEASUREMENTS AND DISCUSSION OF THE RESULTS

In this section we present the results of applying the measurement procedure described in the previous two sections to a variety of other plates. We then examine these results to see what they reveal about the physical differences between the plates. The measured constants for all five plates (including the plywood plate already discussed) are summarised in Table 5. The  $D$ s were determined as in case A of Table 2. The detailed measurements and predictions of frequencies and  $Q$ -factors are given in Tables 6–9. The appropriate points for all five plates are marked in Fig. 4, labelled 1–5 corresponding to Table 5. After making some general remarks relevant to all the

Table 5. Physical parameters for the five boards tested: (1) the plywood plate discussed in detail in Sections 3 and 4; (2) glass-fibre-reinforced resin printed circuit board material; (3) unidirectional carbon fibre laminated on both sides of a light core; (4) quarter-cut Norway spruce (*Picea abies*); and (5) Norway spruce cut with a ring angle about 40° to the plate normal. Values for  $\eta_2$  are quoted only for certain plates, for which it proved possible to make a realistic estimate

Plate	1	2	3	4	5
$a$ (mm)	225	150	204	178	190
$b$ (mm)	225	177	204	178	170
$h$ (mm)	6.36	3.23	1.18	2.40	2.26
$\rho$ (kg/m <sup>3</sup> )	674	2081	687	415	399
$D_1$ (MPa)	986	2840	5570	1320	880
$D_2$ (MPa)	15	1200	560	77	24
$D_3$ (MPa)	411	2560	543	82	13
$D_4$ (MPa)	233	2470	884	227	229
$\eta_1$	0.0105	0.0031	0.0020	0.0051	0.0074
$\eta_2$	—	0.0047	—0.0061	—	—
$\eta_3$	0.0128	0.0033	0.0113	0.0216	0.0212
$\eta_4$	0.0239	0.0070	0.0154	0.0164	0.0139

Table 6. Measured and predicted frequencies and  $Q$ -factors for plate 2 of Table 5, of printed circuit board material

Mode		Measured frequency	Best predicted frequency	Measured $Q$	Predicted $Q$ , "A"	Predicted $Q$ , "B"	$J_1$	$J_2$	$J_3$	$J_4$
1		243	243	160	149	146	0.019	0.002	0.032	0.948
2		396	395	316	279	320	0.094	-0.124	1.030	0.003
3		600	598	320	307	315	0.962	0.005	0.030	0.003
4		632	635	176	187	185	0.030	-0.017	0.422	0.565
5		760	762	225	207	219	0.608	-0.048	0.057	0.384
6		1113	1119	275	308	301	0.018	-0.014	0.989	0.007
7		1244	1234	179	187	182	0.250	0.024	0.136	0.591
8		1310	1323	207	226	231	0.048	-0.046	0.706	0.293
9		1624	1634	285	295	321	1.008	-0.031	0.017	0.006
10		1780	1799	237	259	266	0.820	-0.003	0.025	0.158
		378	376	380	253	346	0.614	-0.230	0.614	0.001
		444	441	341	345	294	0.446	0.103	0.446	0.005









Cases "A" and "B" of the  $Q$ -factor predictions are explained in the text. The factors  $J_1$ ,  $J_2$ ,  $J_3$  and  $J_4$  are also given. The diagrams of mode shapes are schematic only, and do not reproduce the plate proportions or the details of the true mode shapes. In fact, for this particular plate the ring and X modes were obtained with an approximately square plate, while the other modes were obtained with a rectangular plate, so that the diagrams are perhaps a little misleading.

Table 7. Measured and predicted frequencies and  $Q$ -factors for plate 3 of Table 5, the carbon-fibre laminated plate with a balsa-wood core

Mode		Measured frequency	Best predicted frequency	Measured $Q$	Predicted $Q$	$J_1$	$J_2$	$J_3$	$J_4$
1		59	59	68	66	0.008	0.000	0.039	0.954
2		89	89	96	84	0.025	-0.050	1.024	0.002
3		148	150	79	72	0.014	-0.007	0.375	0.618
4		244	244	84	84	0.053	-0.062	1.000	0.009
5		286	286	484	442	1.005	-0.017	0.011	0.002
7		316	312	206	249	0.822	0.011	0.031	0.136
8		389	388	126	131	0.547	0.005	0.089	0.360
		262	269	92	118	0.572	-0.144	0.572	0.000
		293	302	167	178	0.458	0.080	0.458	0.003

The factors  $J_1$ ,  $J_2$ ,  $J_3$  and  $J_4$  are also given. Notice that mode 6 was not measured for this plate. The diagrams of mode shapes are schematic only, and do not reproduce the plate proportions or the details of the true mode shapes.

Table 8. Measured and predicted frequencies and  $Q$ -factors for plate 4 of Table 5, a quarter-cut plate of Norway spruce of suitable quality for instrument making











Mode	Measured frequency	Best predicted frequency	Measured $Q$	Predicted $Q$	$J_1$	$J_2$	$J_3$	$J_4$
1 	102	102	59	60	0.007	-0.001	0.043	0.949
2 	119	119	40	42	0.012	-0.026	1.012	0.001
3 	245	240	57	55	0.014	0.001	0.277	0.708
4 	335	328	46	42	0.014	-0.025	1.008	0.003
5 	479	480	140	136	1.001	-0.010	0.009	0.001
6 	522	523	117	120	0.843	-0.001	0.010	0.145
	459	460	51	54	0.548	-0.097	0.548	0.000
	498	499	81	84	0.467	0.065	0.467	0.001

The factors  $J_1$ ,  $J_2$ ,  $J_3$  and  $J_4$  are also given. The diagrams of mode shapes are schematic only, and do not reproduce the plate proportions or the details of the true mode shapes.

measurements, we then go through the plates in turn, describing them and drawing individual conclusions.

There are two general remarks to be made. First, the simple thin-plate bending theory is quite well supported by all measurements. Both frequencies and damping factors are matched to reasonable accuracy by the best predictions in each case. For the frequency predictions this is perhaps not surprising,

Table 9. Measured and predicted frequencies and  $Q$ -factors for plate 5 of Table 5, a plate of Norway spruce cut with a ring angle of about 40°, but sold as being of suitable quality for instrument making

Mode	Measured frequency	Best predicted frequency	Measured $Q$	Predicted $Q$	$J_1$	$J_2$	$J_3$	$J_4$
1 	50	50	38	46	0.010	-0.022	1.011	0.001
2 	93	93	65	72	0.010	0.002	0.029	0.959
3 	138	138	46	47	0.007	-0.016	1.008	0.002
4 	193	194	69	69	0.024	0.007	0.110	0.859
5 	267	270	52	47	0.014	-0.017	1.001	0.002
6 	310	314	73	66	0.027	0.010	0.230	0.732
7 	331	331	134	134	0.992	0.001	0.007	0.000
8 	391	380	109	109	0.752	-0.006	0.017	0.237
	405	404	—	—	—	—	—	—
	437	435	—	—	—	—	—	—

The factors  $J_1$ ,  $J_2$ ,  $J_3$  and  $J_4$  are also given. For this particular plate, the ring and X mode  $Q$ -factors were not measured, so no damping data are given. The diagrams of mode shapes are schematic only, and do not reproduce the plate proportions or the details of the true mode shapes.

although detailed experimental checks on orthotropic plate theory are not very common. For internal damping, this is believed to be the first systematic test of the theory used here [15], and the level of agreement revealed is broadly satisfactory. Incidentally, notice that the values of the  $J$ s given in association with the various results confirm an earlier claim. It is evident that the four  $J$ s do vary independently from specimen to specimen, within the constraint of equation (11), which proves that all four elastic constants  $D_1$  to  $D_4$  are indeed necessary, independently, to predict mode frequencies accurately. This contrasts with a view sometimes expressed that since only three independent combinations of the  $D$ s enter the equation of motion for a uniform plate, equation (4), the fourth constant is not relevant. As remarked earlier and confirmed here, the fourth constant does indeed make a significant contribution via the boundary conditions, even for a uniform plate.

The second general remark concerns the large range of parameters and material types covered by the five plates tested. For example, the ratio of bending stiffnesses in the two principal directions,  $D_1:D_3$ , ranges from almost unity (plate 2) to nearly 70:1 (plate 5). Similarly, the plate materials range from wood (plates 4 and 5), through a traditional composite (plywood, plate 1), to more modern composites (plates 2 and 3). Plate 2 is the familiar material used for printed circuit boards, a resin matrix reinforced by a rectangular array of glass fibres. Plate 3 is an experimental material, arising from preliminary efforts to design a composite material which might match the properties of spruce for musical instrument soundboards. It has a "sandwich" construction, with unidirectional carbon fibres on both outer surfaces enclosing a light core material, balsa wood.

### 5.1. Plate 2 (circuit board material)

The detailed results for plate 2 are given in Table 6. The columns of measured and predicted frequencies require no explanation, since they were obtained in precisely the same way as in case A of Table 1 discussed in Section 3. The damping results do, however, require some comment. The column headed Predicted  $Q$ , "A" is the result of carrying out the least-squares fitting process described in Section 4, but not including  $\eta_2$  (i.e. holding  $\eta_2 = 0$ ), and not including the ring and X mode measurements in the set to be fitted. It will be seen that the modes other than the ring and X modes are fairly well matched by this process, but the X mode is very poorly predicted and the relative magnitudes of the X and ring  $Q$ -factors are not even the right way round. In the column headed Predicted  $Q$ , "B" the process has been repeated with  $\eta_2$  and the ring and X mode  $Q$ s included. It is reassuring that the values of  $\eta_1$ ,  $\eta_3$  and  $\eta_4$  are left essentially unchanged. The value for  $\eta_2$  produced is that given in Table 5. The ring and X mode  $Q$ s are still not fitted as well as the other modes,

but the predictions are now closer on the whole. In particular the relative magnitudes of the ring and X mode  $Q$ s are now essentially correct.

Thus for this plate we have obtained a significantly non-zero value for  $\eta_2$ , albeit probably less accurate than the values for the other three  $\eta$ s. The reason we could do this here, while it was not possible at all for plate 1, lies in the values of  $J_2$  listed in Tables 3 and 6. The largest value of  $J_2$  in Table 3 is 0.003, whereas the largest value in Table 6 has magnitude 0.230. The implication is that for the plywood plate,  $\eta_2$  had negligible effect on the modal damping factors, whereas for the printed circuit board it has a significant influence so that we were able to carry out the fitting procedure just described with some hope of success. A similar pattern will be revealed by the other plates to be discussed: plate 3 gave sufficiently large values of  $J_2$  to make an estimate of  $\eta_2$  possible, while plates 4 and 5 did not.

Since for plate 2 the values of  $D_1$  and  $D_3$  turned out to be almost equal, one might be tempted to suppose that this plate behaves approximately isotropically. However, comparison with equations (17) will show that this is not the case. If we take the average value of  $D_1$  and  $D_3$ , combine it with the value of  $D_2$ , and use the first three of equations (17) to deduce a Young's modulus and a Poisson's ratio, we obtain  $E \approx 31$  GPa and  $\nu \approx 0.22$ . The last of equations (17) would then predict  $D_4 \approx 4.2$  GPa, which is greater than the measured value (2.47 GPa) by a significant factor of 1.7. Certain mode frequencies predicted on the basis of isotropic theory would thus be in error by some 30% for this plate, a fact which could have serious consequences when designing for vibration control in practice.

It is not hard to see the physical reason for the anisotropy. The reinforcing fibres run parallel to the  $x$  and  $y$  directions, and serve to increase the values of  $D_1$  and  $D_3$  relative to the values which would apply to the resin matrix alone. If there are roughly equal numbers of fibres running in the two directions, one would still expect  $D_1$  and  $D_3$  to be approximately equal. However,  $D_4$  is proportional to the in-plate shear modulus, and this will be very little influenced by the reinforcing fibres. In a pure shearing motion of the relevant type the fibre directions will be rotated but not extended to leading order, so that the fibres will not be stretched. The shear modulus will thus be close to that of the resin matrix alone, much lower than would be calculated on the assumption of isotropic theory using the stiffened values of  $D_1$  and  $D_3$ , exactly as we have just seen.

It seems quite possible that the procedure described here for measuring the elastic and damping constants of orthotropic plates could play a useful role in the non-destructive testing of built-up plates like those used to make printed circuit boards. One might well imagine that any faults in the fabrication process would change the values of the  $D$ s or the  $\eta$ s. If a batch of nominally identical boards were tested by

the procedure outlined, such faults might thus show up as characteristic variations in the measured values. One can imagine automating the procedure, and it could then contribute usefully to quality control.

There is one final observation to be made on the results for plate 2, when compared with those for plate 1. In a general way, one could describe both materials as having a rectangular array of "fibres" set in a "matrix"—for plate 1, these are the wood fibres (predominantly cells called *tracheids*, which run vertically in the tree, sparsely interspersed with *rays*, which run radially in the tree [16]) set in an amorphous inter-cell medium consisting mainly of lignin. The two sets of results are, however, less similar than this analogy might suggest. In particular, the very small value for the ratio  $D_2:D_3$  for plate 1 contrasts strongly with the much larger value for plate 2, as shown in Fig. 4.

The reason is to be found in the fact that the glass fibres stiffening plate 2 are solid, while the wood fibres are hollow tubes. As explained earlier,  $D_2/D_3$  determines a Poisson's ratio. For plate 2, both the resin and the glass have broadly similar values of Poisson's ratio, so that the composite plate has a similar value, around 0.22 as suggested above. For the plywood, though, the corresponding Poisson's ratio is tiny—around 0.02. This small value is of the same order as published values of  $\nu_{RL}$  or  $\nu_{TL}$  for appropriate woods [1], and results from the fact that if a thin-walled tube is compressed or extended across its cross-section, the deformation consists mainly of bending in the tube walls, and necessitates very little Poisson extension or contraction along the length of the tube [8, 17]. The tubes furthermore have relatively great longitudinal stiffness. These factors combine with the laminated construction of plywood to produce a small in-plane Poisson's ratio for the overall behaviour of the plate, as seen in the measurements given here.

### 5.2. Plate 3 (carbon fibre sandwich)

Perhaps the first thing to say about plate 3, the carbon fibre composite plate, is that it is not *a priori* clear that thin-plate bending theory should apply at all to this sandwich construction, with outer layers of extremely high modulus laminated onto a soft core. However, the results for both frequencies and damping factors given in Table 7 strongly suggest that the theory is in fact applicable, at least in the frequency range covered by these measurements.

The results require no special comment in this case: the procedures of Sections 3 and 4 have been followed to produce sets of best-fitted elastic and damping constants. As with plate 2, the values of  $J_2$  for this plate proved sufficiently large to obtain a meaningful estimate of  $\eta_2$ . Notice that in this case the estimate turns out to be negative, whereas the estimate given for plate 2 was positive. This poses no problems:  $\eta_2$ , as with  $J_2$ , can take either sign, as can  $D_2$ . This is not the case for the other constants. It is obvious from the

definitions (10) that  $J_1$ ,  $J_3$  and  $J_4$  are positive, and the fact that the three simple modes discussed earlier more or less isolate the effects of  $D_1$ ,  $D_3$  and  $D_4$  respectively, and  $\eta_1$ ,  $\eta_3$  and  $\eta_4$  respectively, forces all six of those constants to be positive (since elastic energy and damping are obviously both positive for every mode). However, no possible motion of the plate can give a non-zero value of  $J_2$  without  $J_1$  and  $J_3$  also being non-zero, from equations (10), so this argument cannot be applied to  $D_2$  and  $\eta_2$ . (In anisotropic materials, negative Poisson's ratios are perfectly possible [18].)

It is interesting to compare the results for this plate with the measurements of Haines *et al.* [19] on a plate of somewhat similar material (they used cardboard rather than balsa as a core material). Those authors did not measure the complete set of eight constants as we have done, but they give sufficient data to reveal a strong contrast in at least one respect. In trying to duplicate the anisotropic properties of quarter-cut spruce, they had difficulty finding a core material which was sufficiently light, yet which did not give excessive internal damping. While the plate measured here did not result from such a careful attempt to reproduce particular properties, it is interesting that no such problem was encountered—rather the opposite. Notice that the  $Q$ -factor of the "long-grain" bar mode, mode 5 in Table 7, is nearly 500, far greater than the 130 or so typical of spruce [10–12]. If one wished to pursue further the possibilities of this material for use in musical instruments, it would be easy to add extra damping to bring the  $Q$ s down to values more typical of spruce.

Finally, it should be noted that the elastic constants for this plate are not as different from those of spruce as might appear at first glance, comparing with plate 4 in Table 5. The definitions of the  $D$ s are perhaps a little misleading here—for a composite material, introducing such concepts as actual thickness and effective volume density is rather artificial. A more useful comparison between plates 3 and 4 for this purpose involves comparing the elastic and kinetic energies per unit area of plate, absorbing the factors of  $h^3$  and  $h$  into the numbers compared. On that basis, the values are not so very different. There seems to be every possibility that a slightly refined design of plate along similar lines could produce something worth a serious test as a musical instrument soundboard. As good spruce becomes increasingly expensive (especially as a result of recent damage to forests in industrialised countries), a synthetic replacement becomes more attractive.

### 5.3. Plates 4 and 5 (spruce)

Plates 4 and 5 are best discussed together. They are both of Norway spruce (*Picea abies*), traditionally used for instrument soundboards. Plate 4 is an example of the preferred quarter-cut plate, while plate 5 is very far from being quarter-cut, having a ring angle of about 40°. The two specimens are



not closely related, having been obtained through standard commercial channels at different times. But both have a similar ring spacing, and it is not inappropriate to compare the broad trends in the measured results with the qualitative behaviour shown in Fig. 1 from Section 2. The results for mode frequencies and  $Q$ -factors are given in Tables 8 and 9, and require no special comment, except to note that for plate 5, modes 1 and 2 have swapped places.

The qualitative comparison of the values of  $D_1$ ,  $D_2$ ,  $D_3$  and  $D_4$  from Table 5 with Fig. 1 (at the appropriate ring angles of 0 and 40°) is encouraging, bearing in mind that Fig. 1 is based on quite different measured data together with the three-dimensional orthotropic theory leading to equations (20)–(24). The only significant deviation is the value of  $D_2$  for plate 5, which is perhaps twice as big as the graph would indicate. This is the least well-determined constant for the most extreme plate measured here (with nearly 70:1 bending stiffness ratio  $D_1:D_3$ ), so perhaps some deviation here is to be expected. Further measurements would be needed to establish whether this indicates a significant shortcoming of the theory, or whether the deviation lies within the sample-to-sample scatter limits for different specimens of such plates (or indeed whether the present measurements or the published data on which Fig. 1 was based are in error). There appears to be some hope of shedding light on this point, and indeed on other aspects of these results for wood, by analysing the microstructural mechanics of the wood [8], but we do not pursue that possibility here.

A final small point to note about these two plates is that the damping constants are very similar between the two plates, much more so than the elastic constants. Damping is of great importance in musical instrument design, even more than in other areas of plate vibration analysis, and so further measurements on this topic would be of great value. Here again, it is possible that microstructure modelling could shed light on the physics of damping in plates cut in different ways from solid timber.

## 6. ERRORS AND ACCURACY ESTIMATION

In this section we examine the various sources of error in the measurement procedure described above, so that a realistic estimate of accuracy can be made in any particular case. This discussion should also indicate the areas in which one might think of taking special pains with the measurements if the maximum possible accuracy is called for. Sources of error can be divided into three classes. First, there are errors arising from faulty experimental technique, which to a large extent we have dealt with in Sections 3 and 4 in describing how the measurements should be made. Second, there are errors associated with departures of the material from the assumed uniformity, about which very little can be done. Finally, there are errors arising from departures from thin-plate bending

theory, which can sometimes be estimated and thus compensated for, up to a point.

There are two sources of error associated with experimental technique: instrumentation and plate supports. For the damping measurements, some kind of transducer to measure the plate motion is needed, and given the difficulties of supporting a "free" plate, a contacting transducer is in many ways simplest. We used a small accelerometer (Bruel and Kjaer type 8307), which inevitably introduces some added mass and probably some added damping. This must be minimised; the best guide is simply to move the transducer around and observe the changes in frequencies and damping factors—the highest frequency and the highest  $Q$  will always be the best. There might be scope for improvement in this area by using different transducers, but we have not explored the possibility.

Similar problems arise from supporting the plate. We have suggested two approaches, small foam blocks for frequency measurements by Chladni patterns, and thread through a hole positioned on a node line for damping measurements. Neither of these is ideal, although both work well enough if sufficient care is taken. The best check on results here is to compare frequencies measured by Chladni patterns with frequencies determined during the damping measurements, with the different support method. If the same answers are obtained, the credibility is greatly increased. As in the discussion above of transducer effects, the highest  $Q$  is always the most believable. In this case, however, there is no simple rule for frequencies—plate supports may contribute both mass and stiffness, so the frequency might be lowered or raised.

Beyond that, error control is largely a matter of careful attention to detail. Both the foam blocks and the thread holes must be very accurately positioned on node lines. At least some of the plates measured here are sensitive to temperature and humidity, so it is important to determine the node lines, drill the holes and take the damping measurements in a constant environment: by the following day the weather may have changed and the node lines moved. It is worth allowing plates to acclimatise to the typical laboratory environment for a while before starting. If a plate is brought in from elsewhere and immediately measured, it is quite common to find the  $Q$ -factors changing steadily as the measurements proceed, as the plate dries out in a heated room.

The second general source of error is deviation of the material properties from the assumed uniformity. The most obvious examples are inhomogeneity of growth or fabrication (such as were noted in Section 3 when discussing the plywood plate), and residual stresses. These effects cannot easily be estimated, and in any case we probably do not want to allow for them—we are seeking average values over the plate of the elastic and damping constants. The low-frequency modes studied here will give some kind

of averaging effect, but the different modes will yield differently-weighted averages so that the inhomogeneities will appear in the results as scatter of measured frequencies and  $Q$ -factors relative to predicted ones. The "best-fitting" approach which we have adopted for both frequencies and  $Q$ -factors will help to an extent, by implicitly performing a further averaging operation over the results for the different modes. Beyond that we cannot usefully go; it seems best simply to use the residual scatter in the results as a measure of the magnitude of the problem, and thus of the accuracy of the measured constants. A related experimental check on accuracy comes from the process of adjusting the plate's aspect ratio to produce the ring and X modes. Sometimes this aspect ratio will not agree with the best-fitted ratio  $D_1/D_3$  according to equation (28). This problem seems to be most marked with plates that are a long way from square. It is not clear from the present work whether it is to be put down to effects under this heading or to those under the next heading.

The third class of errors consists of departures of the plate behaviour from the assumed theory, of a type which we might be able to estimate. Under this heading come shear and rotatory inertia corrections, edge effects, and effects of air loading. Also, for some composite plates such as our plate 3, there is the question of whether conventional bending theory is applicable in the first place when the plate has very large variations of properties through its thickness, for instance when cross-plane shear moduli are relatively small in the case of a sandwich construction like plate 3. This last question we shall not go into further—we have noted that our measurements do in fact agree quite well with the predictions of bending theory, and we shall be content with that pragmatic answer. The theory of composite materials is a rapidly-developing field, and many studies of relevant problems can be found in the literature.

We will, however, address the other effects briefly. Estimates are available for shear, rotatory inertia and edge corrections, and a (much cruder) estimate can easily be given for air loading. There is an important reason for treating these effects separately from the effects of inhomogeneity discussed above. In that latter case, we were able to argue that the errors were to some extent random, so that the experimental procedure gave some hope of averaging them out. The effects now under discussion, by contrast, are systematic, all tending to reduce mode frequencies and thus to lead to underestimated elastic constants when interpreted by uncorrected bending theory, the more so for the higher modes. This tendency seems to be noticeable in the results for the thickest plate, Table 1.

The general nature of the leading-order corrections for shear, rotatory inertia and edge effects can be seen from the expressions for the special case of a plate cut from an isotropic solid. The three corrections each appear in the form of extra contributions to the

energy integrals (1) and (2). Shear, and associated effects at the same order of approximation, require an extra potential energy term [14, paragraph 304]

$$\frac{Eh^5}{480(1-\nu)(1-\nu^2)} \times \iint \left\{ 4|\nabla(\nabla^2 w)|^2 + (8+\nu) \times \left[ (1-\nu) \left( w_{xx} \frac{\partial^2}{\partial x^2} + 2w_{xy} \frac{\partial^2}{\partial x \partial y} + w_{yy} \frac{\partial^2}{\partial y^2} \right) (\nabla^2 w) + \nu \nabla^2 w \nabla^4 w \right] \right\} dA. \quad (32)$$

Rotatory inertia and associated inertial effects at the same order require an extra kinetic energy term

$$\frac{\rho h^3 \omega^2}{24} \iint \left\{ \frac{\nu}{1-\nu} w \nabla^2 w + |\nabla w|^2 \right\} dA. \quad (33)$$

Finally, the edge correction for a free, square-cut edge requires an extra potential energy term in the form of a line integral around the edge of the plate. For our case of a plate with straight edges parallel to the  $x$  and  $y$  axes, this takes the very simple form [20]

$$-\frac{CEh^4}{2(1+\nu)} \oint w_{xy}^2 dl \quad (34)$$

where

$$C = 16 \sum_{n=0}^{\infty} \frac{1}{[(2n+1)\pi]^5} = 0.05252.$$

The computer program described in the Appendix lends itself to incorporating these corrections very easily, to yield a program which gives results for rectangular, isotropic plates which are formally correct to  $O(h/a)^5$ . The corrections given above should be incorporated in a perturbation sense, solving the thin-plate problem then evaluating the corrections with each unperturbed mode shape and recalculating the frequency. Numerical convergence problems arise if the corrected energy expressions are incorporated *before* calculating eigenvectors and eigenvalues, as will be discussed further in the Appendix.

Unfortunately, things are less simple for orthotropic plates. For the simplest case of a plate cut in a principal plane of an orthotropic solid, the expressions corresponding to equations (32)–(34) would not be enormously complicated, but they would be of very limited use to us. The problem is that they would bring in more independent elastic constants in addition to the four we have already. Since our aim is to *determine* elastic constants, a correction which brings in further unknown constants does not help very much. The problem does not arise in the isotropic case, of course, because for that case only two constants are needed, and both already appear in the thin-plate theory.

It thus appears that for orthotropic plates, we can use the corrections only to estimate the magnitude of

the various effects roughly, and perhaps to give an *ad hoc* correction to the elastic plate constants using plausible typical values of the other constants. For these purposes, the isotropic expressions (32)–(34) give a useful qualitative guide. When applied to a plate cut from an orthotropic solid, the moduli which are relevant to these corrections include the shear moduli through the thickness of the plate, and the cross-plane compression modulus and Poisson's ratios. It should be borne in mind that for some of the materials tested here, these shear moduli in particular might be much smaller than the in-plate shear modulus related to  $D_4$ , as was noted at the end of Section 2 for the case of wooden plates. This could have the result that shear corrections might come into play much sooner than would be the case for isotropic material.

Much the same can be said about the effects of air loading. A very rough estimate of that (for modes below the coincidence frequency [21]) would be to add extra kinetic energy corresponding to the mass of air within a volume surrounding the plate out to a distance of perhaps  $\pi^{-1}$  times a half-wavelength of bending. If that mass of air is not negligible compared with the total mass of the plate, air loading may have a significant effect. One could, of course, think of removing this particular problem by measurements *in vacuo*. That course of action is not without difficulties, however. First, the experimental methodology would have to be modified—a loudspeaker does not make a very good exciter in a vacuum. Second, we have already noted that at least some of the plates tested here (in particular the wooden ones) are sensitive to humidity. To put such a plate in a vacuum is likely to have a desiccating effect, which could change the behaviour significantly. Even so, there might be cases where it would be worth pursuing this possibility.

## 7. CONCLUSIONS

A simple method for measuring all four elastic constants and at least three of the four damping constants for a flat, thin, orthotropic plate has been presented. The method has been illustrated with measurements in the low audio-frequency range on five plates covering a wide range of material types and parameter values. The approach is based on the analysis of frequencies and damping factors of low vibration modes, which makes it suitable for use on many materials for which conventional static or ultrasonic methods cannot be used. The results illustrate, both theoretically and experimentally, the fact that all four constants enter the thin-plate vibration problem independently, even though the thin-plate equation contains only three independent constants in the case of a homogeneous plate. The relative values of the four constants vary substantially from material to material, and the way in which they vary can frequently be understood in terms of the physical

structures of the different materials. For example, a circuit-board composite was found to have nearly equal bending stiffnesses in its two principal directions (the mutually orthogonal directions of the reinforcing fibres) but behaved far from isotropically because, for instance, some orientations of in-plate shear stretch the fibres but others do not.

**Acknowledgements**—The authors are very grateful to Dr J. F. M. Scott for deriving and supplying the correction formulae, equations (32)–(34), to Dr C. M. Hutchins and Professor M. F. Ashby for helpful discussions, and to CIBA-GEIGY Ltd for supplying the carbon-fibre composite plate.

## REFERENCES

1. R. F. S. Hearmon, *The Elasticity of Wood and Plywood*. Forest Products Research Special Report No. 7. H.M.S.O., London (1948).
2. R. F. S. Hearmon, *Introduction to Applied Anisotropic Elasticity*. Oxford Univ. Press (1961).
3. L. Filipczynski, Z. Pawlowski and J. Wehr, *Ultrasonic Methods of Testing Materials*. Butterworths, London (1966).
4. V. Bucur and R. R. Archer, *Wood Sci. Technol.* **18**, 255 (1984).
5. D. R. Bland, *Theory of Linear Viscoelasticity*. Pergamon, London (1960).
6. M. E. McIntyre and J. Woodhouse, *J. Catgut Acoust. Soc.* **42**, 11 (1984).
7. M. E. McIntyre and J. Woodhouse, *J. Catgut Acoust. Soc.* **43**, 18 (1985).
8. M. E. McIntyre and J. Woodhouse, *J. Catgut Acoust. Soc.* **45**, 14 (1986).
9. M. E. McIntyre and J. Woodhouse, *Acustica* **39**, 209 (1978).
10. I. Barducci and G. Pasqualini, *Il Nuovo Cimento* **5**, 416 (1948).
11. J. C. Schelleng, *Catgut Acoust. Soc. Newslett.* **37**, 8 (1982).
12. D. W. Haines, *Catgut Acoust. Soc. Newslett.* **31**, 23 (1979).
13. J. W. S. Rayleigh, *The Theory of Sound*, 2nd edn. Macmillan, London (1894); Dover, New York (1945).
14. A. E. H. Love, *A Treatise on the Mathematical Theory of Elasticity*. Cambridge Univ. Press (1927).
15. But note that some relevant data for musical instrument wood has been presented and discussed by G. Caldersmith, *Acustica* **56**, 144 (1984).
16. J. Bodig and B. A. Jayne, *Mechanics of Wood and Wood Composites*. Van Nostrand Reinhold, New York (1982).
17. A. T. Price, *Phil. Trans. R. Soc.* **228A**, 1 (1928).
18. L. J. Gibson, M. F. Ashby, G. S. Schajer and C. I. Robertson, *Proc. R. Soc.* **A383**, 25 (1982).
19. D. W. Haines, C. M. Hutchins, M. A. Hutchins and D. A. Thompson, *Catgut Acoust. Soc. Newslett.* **24**, 25 (1975).
20. J. F. M. Scott, Personal communication.
21. L. Cremer, H. A. Müller and T. J. Schultz, *Principles and Applications of Room Acoustics*, Chap. IV.10. Appl. Sci., Barking (1982).

## APPENDIX

### Computing Plate Modes

When doing the computations for this work, a method of calculating free rectangular plate modes was used which is simpler, more reliable and much easier to code than the method described by us previously [9]. It is based on using

a power series trial function in Rayleigh's method, and it takes advantage of the fact that for the particular case of free boundaries, the boundary conditions need not enter the calculations at all since Rayleigh's principle takes care of them implicitly. We take as our plate displacement function the expression

$$w(x, y) = \sum_n \sum_m a_{nm} x^n y^m \quad (\text{A1})$$

and by simple integration, we express the kinetic and potential energy integrals  $T$  and  $V$  [equations (1) and (2)] as quadratic forms in the coefficients  $a_{nm}$ . Because of the symmetry of the problem, one need only consider a quarter of the plate. With the origin at the plate centre the powers in the  $n$  and  $m$  summations are each taken as either all even or all odd, catering for the four possible cases of symmetry or antisymmetry about the two symmetry axes of the plate. Applying Rayleigh's method in the usual way, we obtain a set of linear equations for the unknown coefficients  $a_{nm}$  which can be solved, for a finite truncation  $m \leq M$ ,  $n \leq N$  of the summations in (A1), simply by calling a suitable eigenvalue-eigenvector routine (we used the NAG library routine F02AEF). Free boundary conditions automatically satisfy themselves in the limit  $M \rightarrow \infty$ ,  $N \rightarrow \infty$  without any effort by the programmer, because free-boundary modes represent unconstrained stationary points of the Rayleigh quotient. (Precisely this fact is also used in the calculus of variations derivation of the explicit forms (5)–(7) of these boundary conditions [e.g. 13, paragraph 215].)

By varying  $M$  and  $N$ , convergence can be tested. For the calculations given here, we used powers up to 11, giving for each symmetry class a  $36 \times 36$  matrix whose eigenvectors and eigenvalues need to be calculated. At this order, no accuracy problems were encountered using double precision arithmetic. Having thus obtained the modes it is easy to calculate the  $J$ s, and these also converged well as  $M$  and  $N$  were increased. The results of this program have been checked against standard textbook results for bars, and against the computations in Ref. [9] which were carried out by an entirely different method (finite differences). They

have also been checked against the simple analytic results which are available for hinged boundaries, the program being forced to implement these boundary conditions by adding potential and kinetic energy terms corresponding to stiff, heavy beams along the edges of the plate.

Having found approximate mode shapes by this method, it is easy to calculate any other auxiliary functions which may be of interest. For example, for the particular case of an isotropic plate, one can readily compute the corrections for shear, rotatory inertia and edge effects as given in equations (32)–(34). As mentioned in Section 6, it is important to calculate these corrections by a perturbation argument, and not to include the extra kinetic and potential energy terms before calculating the eigenvalues and eigenvectors. The reason is somewhat subtle, depending on a careful analysis of how one should deduce boundary conditions from truncated asymptotic expansions such as are represented by the expressions (32)–(34). Globally minimising the Rayleigh quotient with these corrections included results in the program trying to enforce a spurious boundary condition, which can lead to serious numerical problems.

The method described here is undeniably crude, in numerical analysis terms. The kinetic energy matrix is very full, and the problem becomes poorly conditioned if the order is pushed too high. One could think of getting around this by using orthogonal polynomials or beam functions instead of the simple power series for our trial function. However, it is worth noting that such a change would not be without cost. First, it would be significantly harder to calculate such things as the  $J$ s or the correction terms of equations (32)–(34). Second, and perhaps less obvious, is the fact that convergence problems of a different kind might still appear, particularly with beam functions. Free-free beam functions all satisfy  $w_{xx} = 0$  at each end, whereas the second partial derivative normal to an edge of a plate is not zero because of Poisson's ratio effects [equation (5)]. Thus no sum of beam functions can satisfy free boundary conditions exactly, and this would manifest itself in a numerical calculation as a problem of non-uniform convergence near the edges.